**MDPI**

*Article*

# Fabrication and Soft Magnetic Properties of Fe–Si–Cr Composites with Double-Insulating Layers Suitable for High-Frequency Power Applications

Zhenyi Huang [1], Huaqin Huang [2], Hao He [2], Kaixuan Li [2], Zhaoyang Wu [1] and Rui Wang [2],*

[1] School of Metallurgical Engineering, Anhui University of Technology, Maanshan 243002, China; huangzhenyi@ahut.edu.cn (Z.H.); ahutwzy@ahut.edu.cn (Z.W.)
[2] Key Laboratory of Green Fabrication and Surface Technology of Advanced Metal Materials, Ministry of Education, Anhui University of Technology, Maanshan 243002, China; ahuthuanghuaqin@ahut.edu.cn (H.H.); hehao@ahut.edu.cn (H.H.); ahutlkx@163.com (K.L.)
* Correspondence: worry@ahut.edu.cn

**Abstract:** Soft magnetic composites (SMCs) are composed of alloy materials with the core and insulating layers as the shell. These composites exhibit high saturation magnetic sensitivity and low hysteresis loss, making them a promising material for various applications. The investigation of double layers is considered valuable as it can effectively address the issues of low resistivity and high dynamic loss that arise from non-uniform insulating layers in SMCs. In this study, Fe-Si-Cr/$SiO_2$ particles with a core–shell heterostructure were produced via chemical vapor deposition (CVD). The Fe-Si-Cr/$SiO_2$ materials were coated with different weight percentages (1–6%) of sodium silicate (SS). Subsequently, Fe-Si-Cr-based SMCs were synthesized through high-pressure molding and heat treatment. The effect of the SS weight percentage on microscopic changes and magnetic characteristics was investigated. These findings indicated that a concentration of 4 wt% of SS was the most effective at enhancing magnetic characteristics. The resultant SMCs exhibited high resistivity (21.07 mΩ·cm), the lowest total loss ($P_{10 \, mt/300 \, kHz}$ of 44.23 W/kg), a relatively high saturation magnetization (181.8 emu/g), and permeability (35.9). Furthermore, it was observed that the permeability exhibited stabilization at lower frequencies. According to these findings, the combination of CVD and double layers could lead to the further development of SMCs in a variety of applications.

**Keywords:** soft magnetic materials; insulating layers; double layers; magnetic properties

## 1. Introduction

Soft magnetic composites (SMCs) utilize alloy materials as their core and insulating layers as the shell, resulting in notable saturation magnetic sensitivity and minimal hysteresis loss, thus demonstrating their potential in various applications [1,2]. However, SMCs frequently exhibit inadequate resistivity and excessive dynamic loss as a result of their thin and non-uniform coating. Researchers have developed a technique known as "double layers" to address this problem, which involves adding a layer of insulation outside the original insulating layers to improve coating uniformity, limiting the eddy current operation, and lowering dynamic loss. Double-layered SMCs have been shown to improve electrical and magnetic properties in recent investigations. For instance, Zhong conducted research [3] on the development of SMCs that incorporated dual-insulating layers composed of phosphates and silicone resin. The resulting SMCs demonstrated a resistivity of 820 mΩ·cm, a quality factor of 55.6 at a frequency of 5.4 MHz, and an eddy current loss of 196.3 W/kg at 500 kHz. In contrast to SMCs with only a vitreous boron oxide coating, Evangelista's work [4] focused on SMCs with double insulating layers of ZnO nanoparticles and vitreous $B_2O_3$. These SMCs demonstrated synergism between

the layers by reducing dynamic loss by nearly 78% and increasing electrical resistivity by nearly ten times. Furthermore, Taghvaei [5] conducted a study on the magnetic properties of Fe–PO$_4$–polyepoxy SMCs. These findings indicate that the application of a nanocrystalline/amorphous PO$_4^{3-}$ thin layer with superior coverage on the powder surface could enhance surface morphology and effectively decrease eddy current losses by over 50%.

Recent research has indicated that the addition of an extra layer of insulation in double-layer SMCs can enhance their electrical and magnetic properties. However, the impact of the thickness of external coatings on the characteristics of SMCs has not been thoroughly investigated. The impact of different insulating layers on the magnetic characteristics of SMCs is currently the primary focus of research. Nonetheless, it is important to remember that external layers that are too thin may not fill the original gap, while external layers that are too thick may amplify the magnetic dilution effect, ultimately resulting in a lower magnetic phase per unit volume [6]. Therefore, it is important to examine how the thickness of exterior coatings affects the properties of SMCs so that their performance can be optimized.

The influence of sodium silicate (SS) (1 to 6 wt%) on the microscopic changes and magnetic characteristics of Fe-Si-Cr/silicon dioxide nanoshells coated using a chemical vapor deposition (CVD) was examined in this study [7]. The powders were then utilized to create Fe–Si–Cr-based SMCs via high-pressure molding and thermal treatment. According to the study, 4 wt% of SS was the ideal concentration to provide desired magnetic characteristics. The resultant SMCs exhibited high resistivity (21.07 mΩ·cm), the lowest total loss (P$_{10 \text{ mt}/300 \text{ kHz}}$ of 44.23 W/kg), relatively high saturation magnetization (181.8 emu/g), and permeability (35.9). Notably, the permeability stabilized earlier at lower frequencies. These findings offer helpful insights for the design of SMCs with enhanced magnetic characteristics by investigating various combinations of CVD and double layers in several different fields.

## 2. Experimental

### 2.1. Chemicals

Fe-Si-Cr alloys in powder form were purchased from Changsha Tijo Metal Material Co., Ltd. (Changsha, China). These powders were fabricated through gas atomization and had a composition of Si (5.51 wt%) and Cr (4.98 wt%). The average particle diameter of the powders was 50 μm. Zhiyuan Chemical Reagent Co., Ltd. (Tianjin, China) provided tetraethyl orthosilicate (C$_8$H$_{20}$O$_4$Si, 99.0%). Henan Yixiang New Material Co., Ltd. (Yixiang, China) supplied the SS (Na$_2$O·nSiO$_2$, n = 3.31). Ar gas with a purity of 99.99% was purchased from Tianze Gas Co., Ltd. (Nanjing, China).

### 2.2. Synthesis

Here, Fe-Si-Cr/SiO$_2$ core–shell powders were created utilizing the CVD process, with silicon dioxide serving as the shell and Fe-Si-Cr serving as the core. The CVD procedure was carried out through the utilization of a mesh sieve with 30 μm wide apertures, where powdered Fe-Si-Cr was placed and subsequently fluidized with argon within a vertical tube oven. Tetraethyl orthosilicate was placed in an oven and heated to 940 K for 60 min while being continuously surrounded by an argon flow at a rate of 300 mL/min. Fe-Si-Cr/SiO$_2$ nanoshells were subsequently subjected to coating with SS solutions of different weight percentages (ranging from 1% to 6%). This was achieved by immersing the nanoshells in a heated graphite die containing an SS solution at 342 K for 30 min, followed by stirring the solution at 50 r/min and drying the coated particles at 90 K for 3 h. After this, the coated particles underwent uniaxial compression at a pressure of 1200 MPa, resulting in the formation of toroidal cores with the following dimensions: outer diameter = 26.9 mm, inner diameter = 14.5 mm, and height = 4.0 mm. To remove any remaining stress, the compacted cores were then tempered at 773 K for 1 h in an argon environment.

### 2.3. Characterization

Various methods were used to investigate the properties of as-synthesized SMCs. X-ray diffraction (XRD) using Cu K$\alpha$ radiation (Bruker D8 Advance, 2°/min) was used to analyze the solid-state structure of the SMCs. The morphological characteristics and local chemical homogeneities were examined with a scanning electron microscope (SEM, Tescan MIRA3 XMU) and energy-dispersive spectroscopy (EDS, JED-2300). Fourier transform infrared reflection (FTIR) spectroscopy was employed on a Nicolet IS 10 spectrometer to analyze the composition of SMCs. X-ray photoelectron spectroscopy (XPS, PHI-5000versaprobe) was used to analyze changes in the electronic structure of SMCs. Under normal industrial conditions, the magnetic properties of SMCs were investigated using a B-H curve analyzer (SY-8258 IWATSU). A vibrating sample magnetometer (MPMS-3) with a step size of 50 Oe was used at 298 K to explore hysteresis loops throughout a magnetic field range of −20,000 to 20,000 Oe. The specific resistance of the SMCs was measured using a ST2253y resistivity tester.
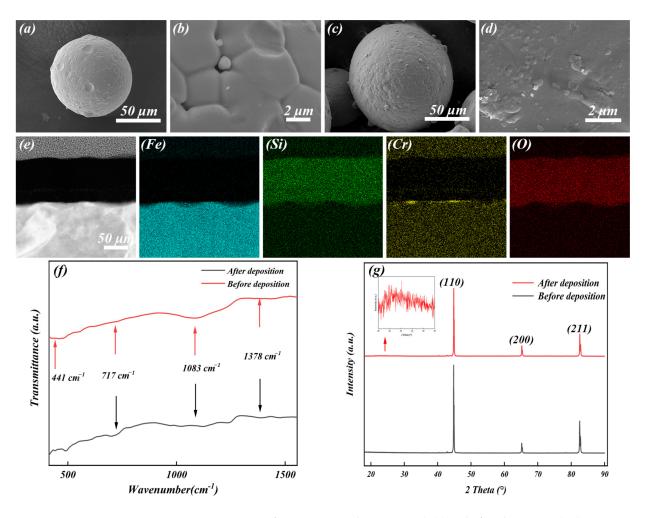
## 3. Results and Discussion

### 3.1. Microstructures of Fe–Si–Cr/SiO$_2$ Core-Shell Materials

To analyze the structural properties of the layered Fe-Si-Cr materials, data from SEM and EDS were obtained both before and after CVD, as depicted in Figure 1a–d. Although aerosolization may cause some surface irregularities such as cavities and bumps, the Fe-Si-Cr particles demonstrated a relatively smooth surface, as illustrated in Figure 1a,b. In addition, Fe-Si-Cr SEM images revealed a continuous and thick SiO$_2$ layer covering the surface of the Fe-Si-Cr base material, resembling a thin film (Figure 1d). Transmission electron microscopy was employed to map the SEM images and EDS spectra of the cross-sections of Fe-Si-Cr/SiO$_2$ powders, as depicted in Figure 1e. According to the EDS maps, Si was discovered to be evenly distributed across the composite's cross-section, whereas O was mostly found on the shell, and Cr and Fe were mostly discovered inside the particles. These findings suggest that the aforementioned methods were applicable in the production of Fe-Si-Cr/SiO$_2$ materials with an improved microstructure and core–shell heterojunction characteristics.
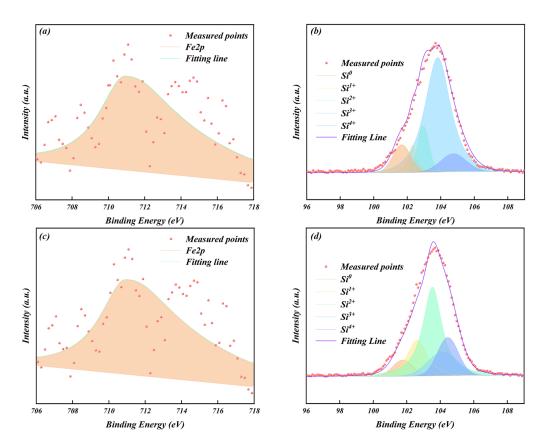
The influence of CVD on the solid-state structure of Fe-Si-Cr materials was investigated using XRD spectroscopy. The findings depicted in Figure 1f indicate the presence of the $\alpha$-Fe(Si, Cr) phase in the body-centered cubic structure of the Fe-Si-Cr alloy and in its raw form. This was verified by the detection of three diffraction peaks at 2θ = 44.73°, 65.12°, and 82.48°, which correspond to the (110), (200), and (211) crystal planes, respectively, in accordance with the JPCDS standard card 06-0696. According to an earlier study, SS deposition caused the production of an amorphous phase with XRD peaks at 2θ between 22° and 28°, showing that SiO$_2$ deposition did not change the phase structure of the Fe-Si-Cr powder [8,9].

FTIR is a widely used analytical technique that enables the determination of molecular structure and the identification of compounds based on the relative vibration and rotation of molecules within substances. Figure 1g displays the impact of CVD on the FTIR data of Fe-Si-Cr. The appearance of three typical IR peaks, at 441 cm$^{-1}$ for rocking vibrations, 717 cm$^{-1}$ for bending vibrations, and 1083 cm$^{-1}$ for asymmetrical stretching vibrations, confirmed the existence of Si-O-Si bonds [10–12]. The vibration mode attributed to the deformations of the C-H bond was observed at 1378 cm$^{-1}$ [13]. Si-O-Si vibrations at 717 cm$^{-1}$ and 1083 cm$^{-1}$ were similar, indicating that the raw Fe-Si-Cr materials had undergone slight oxidation. The findings indicate that Fe-Si-Cr/SiO$_2$ composites featuring core–shell heterojunctions were effectively synthesized, wherein the Fe-Si-Cr alloy served as the core and silicon dioxide and as the isolating shell. In addition, it was observed that the solid-state structure of Fe-Si-Cr remained unaltered after the deposition of SiO$_2$.

**Figure 1.** SEM images of Fe–Si–Cr powders prior to (**a**,**b**) and after deposition (**c**,**d**); EDS spectra (**e**), FTIR spectra (**f**), and XRD patterns (**g**).

Changes in Fe-Si-Cr materials before and after CVD were confirmed by XPS analysis, the results of which are shown in Figure 2a–d. The peak positions and atomic ratios were determined through curve fitting. To correct the positions of the other peaks, the electron binding energy of the C1s peak was established at 284.8 eV. Before CVD, the Fe-Si-Cr substrate showed a Fe 2p peak at 710.8 eV (21.38 at%) (Figure 5a), which corresponded to Fe0 [14]. The Fe $2p_{3/2}$ level in the Fe-Si-Cr material exhibited a slightly higher binding energy compared to that anticipated for pure iron, which could be ascribed to the interactions between silicon and chromium [15]. The Si 2p spectrum exhibited multiple peaks that corresponded to various chemical species, including $Si^0$, sub-oxides ($Si^{1+}$, $Si^{2+}$, and $Si^{3+}$), and $SiO_2$ ($Si^{4+}$). Specifically, the peaks observed at 101.67 eV (6.59 at%) correspond to $Si^0$, while those at 102.32 eV (6.98 at%), 102.92 eV (10.46 at%), 103.82 eV (63.73 at%), and 104.75 eV (9.19 at%) correspond to $Si^{1+}$, $Si^{2+}$, $Si^{3+}$, and $Si^{4+}$, respectively. Following the deposition process, the position and fitting outcome remained unchanged. Moreover, the five peaks that corresponded to Si exhibited comparable binding energies: $Si^0$ (101.75 eV, 6.59 at%), $Si^{1+}$ (102.63 eV, 16.69 at%), $Si^{2+}$ (103.53 eV, 45.31 at%), $Si^{3+}$ (104.16 eV, 14.76 at%), and $Si^{4+}$ (104.45 eV, 16.65 at%). The observed decreases in $Si^0$ (31.64%), $Si^{3+}$ (76.84%), and a rise in $Si^{4+}$ (44.80%) could be attributed to the production of $SiO_2$ particles during the CVD process [16]. The results of the XPS analysis confirmed the successful deposition of $SiO_2$ on Fe–Si–Cr powders.
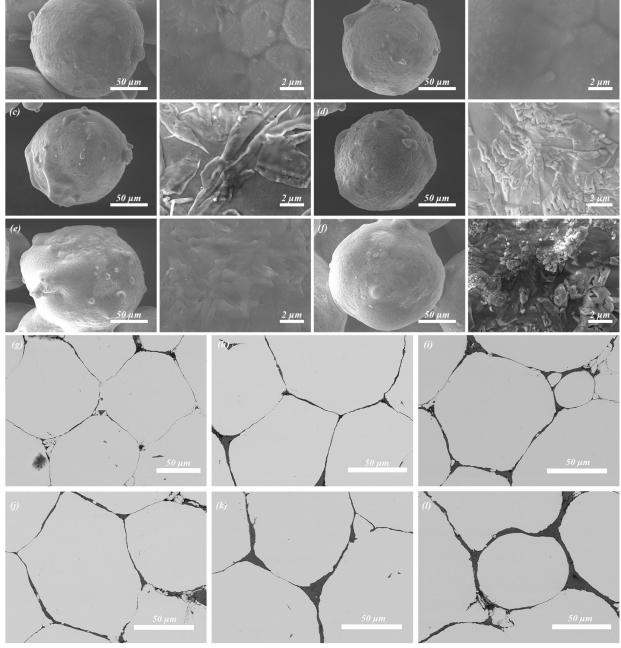
**Figure 2.** XPS results of Fe–Si–Cr composites before ((**a**)–Fe, (**b**)–Si) and after deposition ((**c**)–Fe, (**d**)–Si).

### 3.2. Microstructures and Magnetic Properties of the Alloy Powders and SMCs with Double Layers

Figure 3a–f shows the surface morphologies of composite powders coated with different weight percentages of SS. These findings indicate that the coating process led to a significant reduction in the number of original pits that were present on the surface of the powder. At low coating concentrations, the clusters detected in the nearest region of the sample powder surface gradually covered the entire powder particles to compensate for the pores which were formed during the CVD process, where $SiO_2$ was not attached. With a gradual increase in the SS coating concentration (3~4 wt%), the micron clusters became denser, ultimately resulting in the formation of a film on the surface of the sample. However, the uniformity and compactness of the insulating layers were negatively impacted by a continuous increase in the coating concentration due to the agglomeration of the external matter on the surface; the density changes are shown in Table 1. Figure 2g–l depicts the backscattered electron (BSE) imaging of the Fe-Si-Cr-based SMCs with a smooth surface. The non-uniformity of the insulating layer was noted to occur when the concentration of SS was within the range of 1–2 wt%, with a tendency for convergence at the particle junction. The incomplete SS insulating layer underwent agglomeration due to the high pressure generated during the pressing process. As the concentration of SS increased, the coating achieved greater uniformity. However, the high SS concentration led to a recurrence in the agglomeration of outside material on the particle surface. Therefore, an SS concentration of 4–5 wt% led to the production of complete SMCs with double layers.

**Figure 3.** SEM images of the Fe–Si–Cr composites before (**a**,**g**) and after deposition (**b**–**f**,**h**–**l**).
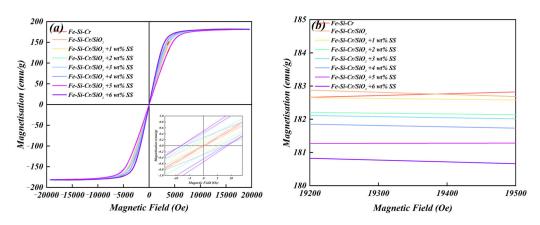
**Table 1.** Density of Fe-Si-Cr-based SMCs with various kinds of insulating layers.

| Sample | Density (g/cm$^3$) |
|---|---|
| Fe-Si-Cr SMCs | $7.11 \pm 0.015$ |
| Fe-Si-Cr/SiO$_2$ SMCs | $7.02 \pm 0.017$ |
| Fe-Si-Cr/SiO$_2$ SMCs with 1 wt% SS | $6.52 \pm 0.017$ |
| Fe-Si-Cr/SiO$_2$ SMCs with 2 wt% SS | $6.43 \pm 0.023$ |
| Fe-Si-Cr/SiO$_2$ SMCs with 3 wt% SS | $6.39 \pm 0.007$ |
| Fe-Si-Cr/SiO$_2$ SMCs with 4 wt% SS | $6.27 \pm 0.012$ |
| Fe-Si-Cr/SiO$_2$ SMCs with 5 wt% SS | $5.85 \pm 0.025$ |
| Fe-Si-Cr/SiO$_2$ SMCs with 6 wt% SS | $5.69 \pm 0.031$ |

Ferromagnetic materials have a characteristic known as saturation magnetization (*Ms*). Ferromagnetic substances exhibit magnetization when subjected to an external magnetic field. Initially, as the external magnetic field intensity gradually increases, the magnetization of the material also increases. The material reaches a state of *Ms* when the external magnetic field reaches a specific intensity, at which point the magnetization of the substance stops rising and stabilizes at a given value. Soft magnetic materials are highly desirable for use in high-power applications due to their notable attribute of possessing a high *Ms*. The hysteresis loops and coercivity of SMCs with varying SS weight percentages are shown in Figure 4. With an increase in the concentration of SS, there was a corresponding increase in the thickness of the insulating layer. Additionally, the rise in the non-magnetic phase resulted in a gradual reduction in the *Ms* of each SMC from 182.9 to 180.6 emu/g. The core–shell model, which could be used to explain the net changes in *Ms* for SMCs, was adopted [17]. This model suggested a significant difference between the magnetic properties of the core and shell materials in SMCs, where "d" and "t" represented the core diameter and the shell layer thickness, respectively, and "v" represented the volume. The total saturation magnetization is given by Equation (1):

$$Ms = (Ms_{(core)}v_{(core)} + Ms_{(shell)}v_{(shell)})/(v_{(core)} + v_{(shell)}) = Ms_{(core)} - 6t(Ms(core) - Ms_{(shell)})/d \quad (1)$$



**Figure 4.** Hysteresis curves of Fe-Si-Cr-based SMCs showing changes in saturation magnetization (**a**) and coercivity (**b**).

The relationship between *Ms* and the net magnetic moment per unit volume indicated that both silicon dioxide and SS exhibited non-magnetic properties [17], resulting in a nearly zero value for $Ms_{(shell)}$ [8,18]. Furthermore, the coercivity exhibited a range of 5 to 10 Oe, whereas the minimum testing steps utilized for hysteresis loop identification were 50, which was considerably higher than the actual value due to equipment limitations. Therefore, coercivity could not be used as the basis for a precise comparison of performance.

Resistivity, which is inversely proportional to conductivity, can be used to accurately characterize the electrical conduction of metal composites. Thicker insulating layers can reduce the scattering centers for electron conductivity per unit volume in metals and enhance resistivity [19]. $SiO_2$ inorganic insulating layers prepared by the CVD method and the SS insulating layers substantially enhanced resistivity, as depicted in Figure 5a. The greater the thickness of the SS insulation layer, the greater the effect of current limiting, which promoted the integrity of the isolating layers and restricted the operation of the vortex between the particles, thereby minimizing subsequent dynamic loss. Permeability is an important index of soft magnetic materials and is also an obvious feature of soft magnetic materials, which are different from permanent magnetic materials. Figure 5b shows how changes in double layers and the SS weight percentage influenced SMC's frequency stability and permeability. In general, the frequency was inversely proportional to the permeability. In addition, at low frequencies, SMCs coated with a higher percentage of SS had lower permeability than SMCs with thinner insulating layers, confirming the

strong magnetic dilution effect of SS coating [20]. This effect increased magnetoresistance by preventing Fe-Si-Cr particles from making electrical contact. In addition, the exchange coupling between the Fe-Si-Cr substrate and the non-conducting layers could result in an efficient surface spin orientation [21]. Nevertheless, when the frequency increased, the permeability of SMCs with thicker insulating layers stabilized at lower frequencies owing to enhanced skin effects [17].
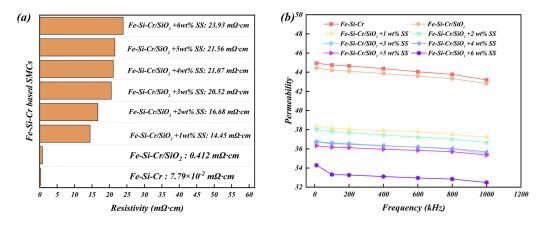


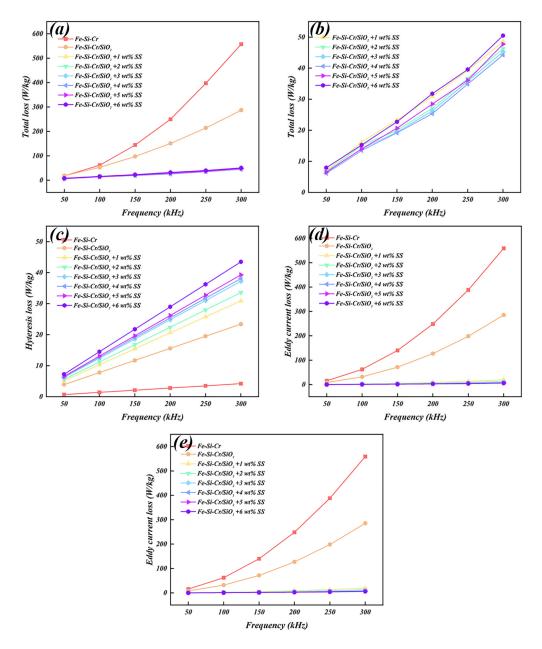**Figure 5.** Trends in the resistivity (**a**) and permeability (**b**) of Fe-Si-Cr-based SMCs.

Core loss can be defined as the power absorbed by the magnetic core in an applied alternating (AC) field, that is, the dissipation of the magnetic core in response to an AC magnetic field. The power in these losses is mostly turned into heat energy, which increases the temperature of the magnetic core, reduces the working efficiency, and even damages the insulation layer. Therefore, the power consumption of Pc is one of the most essential factors to consider when evaluating magnetic materials for AC applications. Figure 6a depicts the distribution of the total loss ($P_{cm}$) of Fe-Si-Cr-based SMCs in a 10 mT external field. $P_{cm}$ values increased with the frequency for all the SMCs. For SMCs with 4 wt% SS addition and uniform insulating layers with superior integrity, the $P_{cm}$ value (44.23 W/kg, measured at 8 kA/m applied field) decreased by 84.6% compared to Fe-Si-Cr SMCs (287.01 W/kg).

As per the classical Bertotti loss separation theory [22], $P_{cm}$ could be separated into two parts: hysteresis loss ($P_{hyst}$, which is defined as the energy absorbed by the material when the AC magnetic field is scanned along the hysteresis loop and can be understood as the energy required to clear the domain walls when magnetized, i.e., the energy required to complete the magnetization) and dynamic loss (when a ferromagnetic material is subjected to an AC magnetic field, the alternating magnetic field causes an induced electromotive force in the material due to electromagnetic induction, and the induced electromotive force causes an induced current in the material, which is often referred to as eddy current). On the one hand, eddy currents create fields that weaken the external magnetic field; on the other hand, eddies can also cause joule loss within the material, and the loss contributed by the eddy current in the total loss of the magnetic core is often referred to as dynamic loss ($P_e$) [19]. Due to the increasing working frequency of electronic equipment, flexible magnetic materials can possess excellent magnetic properties at high frequencies. The hysteresis loss of $P_h$ and dynamic loss of $P_e$ reduce the magnetic properties of the material in the AC field. Therefore, it is very important to reduce these losses with an efficient AC device.

$$P_{cm} = K_h f + K_e f^m \tag{2}$$

Equation (2) shows the dependency of $P_{cm}$ on the dynamic loss coefficient ($K_e$) and the hysteresis loss coefficient ($K_h$). At a fixed magnetic field strength (m = 2), the dynamic loss was proportional to the square of the operating frequency, whereas the hysteresis loss depended linearly on the operating frequency. Initially, the $P_{cm}/f$ vs. $f$ curve was fitted using a linear fitting method, and the fitted curve was extrapolated to the zero-frequency

point to obtain the intercept of the hysteresis loss value under quasi-static conditions, while Equation (2) with the coefficients $K_e$ and $K_h$ constants only had a qualitative value. This result was multiplied by the frequency to obtain the hysteresis loss value at that frequency, as presented in Figure 6c [23]. Subtracting the total loss from the fitted hysteresis loss provided dynamic loss, as depicted in Figure 6d,e. $P_{hyst}$ values increased almost linearly with the frequency for all the Fe-Si-Cr-based SMCs. The excessive thickness of the insulating layers restricted the motion of the domain walls, resulting in a gradual increase in the hysteresis loss with an increase in the SS mass fraction [24]. Moreover, the core–shell heterogeneous structure of Fe-Si-Cr-based SMCs primarily reduced the dynamic loss by improving resistivity and restricting the effective operating diameter of the eddy currents [25]. Therefore, thicker insulating layers were proved to be more efficient at minimizing the dynamic loss in SMCs.



**Figure 6.** Total loss (**a**,**b**), hysteresis loss (**c**), and dynamic loss (**d**,**e**) of SMCs with various insulating layers measured at 10 mT and 50–300 kHz.

Fe-Si-Cr-based SMCs with 4 wt% SS, in addition, showed the most desirable magnetic properties compared to the other samples. The $P_{ec}$ decreased by 69.1%, indicating a significant reduction in dynamic losses, while the $P_{hyst}$ only increased by 23.3%, indicating a smaller increase in hysteresis losses. Thus, 4 wt% was the optimal SS addition concentration that achieved both low total losses and high magnetic properties. The resistivity of SMCs was high (21.07 mΩ·cm), and the total loss (at 10 mT and 300 kHz) was the lowest (44.23 W/kg) compared to other samples. The saturation magnetization was relatively high (181.8 emu/g), and the permeability was 35.9, which stabilized at lower frequencies. Compared with other single inorganic coating layers, such as $FeSiCr/MgO$ SMCs, $FeSiCr/CaO$ SMCs, $FeSiCr/TiO_2$ SMCs, $FeSiCr/ZrO_2$ SMCs, $FeSiCr/SiO_2$ SMCs, $FeSiCr/BaTiO_3$ SMCs, the SMCs with double-layers had higher resistivity, permeability, and lower dynamic loss [26–28]; compared with SMCs with organic coatings, for example, and the FeSiCr SMCs with phosphating layer, our SMCs had lower hysteresis loss [29].

## 4. Conclusions

The objective of this study was to analyze the structural properties of core–shell heterostructures and the magnetic features of Fe-Si-Cr-based SMCs containing different weight percentages of SS additives. The main findings can be summarized as follows.

Firstly, as the SS concentration increased, the core–shell heterostructure became more uniform and well-incorporated, with an optimal concentration being 4–5 wt% for the formation of complete SMCs with double layers. Secondly, increasing the thickness of the SS insulating layers resulted in decreased permeability and saturation magnetization due to magnetic dilution effects, while resistivity and hysteresis loss increased. Finally, at 10 mT and 300 kHz, the SMCs showed the stabilization of permeability at lower frequencies and exhibited a total loss of 44.23 W/kg (an 84.6% reduction), a *Ms* of 181.8 emu/g, and a resistivity of 21.07 mΩ·cm when the SS concentration was 4 wt%, which was the optimal condition among all the samples. The results of this study demonstrate that the combination of CVD and double layers holds promise for advancing the development of SMCs in diverse fields.

## References

1. Liu, D.; Wu, C.; Yan, M.; Wang, J. Correlating the microstructure, growth mechanism and magnetic properties of FeSiAl soft magnetic composites fabricated via $HNO_3$ oxidation. *Acta Mater.* **2018**, *146*, 294–303. [CrossRef]
2. Wu, X.; Ding, J.; Kong, Y.; Sun, Z.; Shao, G.; Li, B.; Wu, J.; Zhong, Y.; Shen, X.; Cui, S. Synthesis of a novel three-dimensional $Na_2SO_4@SiO_2@Al_2O_3-SiO_2$ phase change material doped aerogel composite with high thermal resistance and latent heat. *Ceram. Int.* **2018**, *44*, 21855–21865. [CrossRef]

3. Zhong, X.; Chen, J.; Wang, L.; Li, B.; Li, L. Properties of FeSiAl-based soft magnetic composites with AlN/Al$_2$O$_3$ and hybrid phosphate–silane insulation coatings. *J. Alloys Compd.* **2018**, *735*, 1603–1610. [CrossRef]

4. Evangelista, L.L.; Filho, A.I.R.; Silva, B.S.; Hammes, G.; Binder, C.; Klein, A.N.; Drago, V. Magnetic properties optimization of an iron-based soft magnetic composite coated by nano-ZnO and boron oxide. *J. Magn. Magn. Mater.* **2021**, *539*, 168319. [CrossRef]

5. Taghvaei, A.H.; Shokrollahi, H.; Janghorban, K.; Abiri, H. Eddy current and total power loss separation in the iron–phosphate–polyepoxy soft magnetic composites. *Mater. Des.* **2009**, *30*, 3989–3995. [CrossRef]

6. Wu, Z.; Xian, C.; Jia, J.; Liao, X.; Kong, H.; Xu, K. Formation Process of the Integrated Core(Fe-6.5wt.%Si)@Shell(SiO$_2$) Structure Obtained via Fluidized Bed Chemical Vapor Deposition. *Metals* **2020**, *10*, 520. [CrossRef]

7. Wang, R.; He, Y.; Kong, H.; Wang, J.; Wu, Z.; Wang, H. Influence of sintering temperature on heterogeneous-interface structural evolution and magnetic properties of Fe–Si soft magnetic powder cores. *Ceram. Int.* **2022**, *48*, 29854–29861. [CrossRef]

8. Gemeay, A.H.; Keshta, B.E.; El-Sharkawy, R.G.; Zaki, A.B. Chemical insight into the adsorption of reactive wool dyes onto amine-functionalized magnetite/silica core-shell from industrial wastewaters. *Environ. Sci. Pollut. Res. Int.* **2020**, *27*, 32341–32358. [CrossRef]

9. de Moura, S.G.; Ramalho, T.C.; de Oliveira, L.C.A.; Dauzakier, L.C.L.; Magalhães, F. Photocatalytic degradation of methylene blue dye by TiO$_2$ supported on magnetic core shell (Si@Fe) surface. *J. Iran. Chem. Soc.* **2022**, *19*, 921–935. [CrossRef]

10. Kim, M.T. Deposition behavior of hexamethydisiloxane films based on the FTIR analysis of Si–O–Si and Si–CH$_3$ bonds. *Thin Solid Films* **1997**, *311*, 157–163. [CrossRef]

11. Sun, K.; Feng, S.; Jiang, Q.; Li, X.; Li, Y.; Fan, R.; An, Y.; Wang, J. Intergranular insulating reduced iron powder-carbonyl iron powder/SiO$_2$-Al$_2$O$_3$ soft magnetic composites with high saturation magnetic flux density and low core loss. *J. Magn. Magn. Mater.* **2020**, *493*, 165705. [CrossRef]

12. Tarhan, İ.; Derin, Z.; Erdem, M.A. The study of Middle Bronze Age pottery from Yassıtepe Höyük site in İzmir, Turkey, by FTIR and XRD with chemometrics. *J. Archaeol. Sci. Rep.* **2022**, *42*, 103401.

13. Swamy, S.K.K.; Ramaprasad, A.T. FTIR signal assignment in Chitin using density functional theory calculations—A monomer approximation. *Mater. Today Proc.* **2022**, *66*, 2504–2507. [CrossRef]

14. Lebugle, A.; Axelsson, U.; Nyholm, R.; Mårtensson, N. Experimental and Core Level Binding Energies for the Metals. *Phys. Scr.* **1981**, *23*, 825–827. [CrossRef]

15. Guo, Y.; Jian, X.; Zhang, L.; Mu, C.; Yin, L.; Xie, J.; Mahmood, N.; Dou, S.; Che, R.; Deng, L. Plasma-induced FeSiAl@Al$_2$O$_3$@SiO$_2$ core–shell structure for exceptional microwave absorption and anti-oxidation at high temperature. *Chem. Eng. J.* **2020**, *384*, 123371. [CrossRef]

16. González-Flores, K.E.; Horley, P.; Cabañas-Tay, S.A.; Pérez-García, S.A.; Licea-Jiménez, L.; Palacios-Huerta, L.; Aceves-Mijares, M.; Moreno-Moreno, M.; Morales-Sánchez, A. Analysis of the conduction mechanisms responsible for multilevel bipolar resistive switching of SiO$_2$/Si multilayer structures. *Superlattices Microstruct.* **2020**, *137*, 106347. [CrossRef]

17. Dong, B.; Qin, W.; Su, Y.; Wang, X. Magnetic properties of FeSiCr@MgO soft magnetic composites prepared by magnesium acetate pyrolysis for high-frequency applications. *J. Magn. Magn. Mater.* **2021**, *539*, 168350. [CrossRef]

18. Tajabadi, M.; Rahmani, I.; Mirkazemi, S.M.; Orimi, H.G. Insights into the synthesis optimization of Fe@SiO2 Core-Shell nanostructure as a highly efficient nano-heater for magnetic hyperthermia treatment. *Adv. Powder Technol.* **2021**, *33*, 103366. [CrossRef]

19. Zheng, J.; Zheng, D.; Qiao, L.; Ying, Y.; Tang, Y.; Cai, W.; Li, W.; Yu, J.; Li, J.; Che, S. High permeability and low core loss Fe-based soft magnetic composites with Co-Ba composite ferrite insulation layer obtained by sol-gel method. *J. Alloys Compd.* **2022**, *893*, 663. [CrossRef]

20. Dippong, T.; Levei, E.A.; Leostean, C.; Cadar, O. Impact of annealing temperature and ferrite content embedded in SiO$_2$ matrix on the structure, morphology and magnetic characteristics of (Co0.4Mn0.6Fe2O4)δ (SiO2)100-δ nanocomposites. *J. Alloys Compd.* **2021**, *868*, 159203. [CrossRef]

21. Guan, W.W.; Shi, X.Y.; Xu, T.T.; Wan, K.; Zhang, B.W.; Liu, W.; Su, H.L.; Zou, Z.Q.; Du, Y.W. Synthesis of well-insulated Fe–Si–Al soft magnetic composites via a silane-assisted organic/inorganic composite coating route. *J. Phys. Chem. Solids* **2021**, *150*, 109841. [CrossRef]

22. Nell, M.M.; Schauerte, B.; Brimmers, T.; Hameyer, K. Simulation of iron losses in induction machines using an iron loss model for rotating magnetization loci in no electrical steel. *COMPEL-Int. J. Comput. Math. Electr. Electron. Eng.* **2022**, *41*, 600–614. [CrossRef]

23. Guo, Z.; Wang, J.; Chen, W.; Chen, D.; Sun, H.; Xue, Z.; Wang, C. Crystal-like microstructural Finemet/FeSi compound powder core with excellent soft magnetic properties and its loss separation analysis. *Mater. Des.* **2020**, *192*, 108769. [CrossRef]

24. Qiu, Y.; Wang, R.; He, Y.; Kong, H.; Li, S.; Wu, Z. Effects of axial pressure on the evolution of core–shell heterogeneous structures and magnetic properties of Fe–Si soft magnetic powder cores during hot-press sintering. *RSC Adv.* **2022**, *12*, 19875–19884. [CrossRef] [PubMed]

25. Zhang, Q.; Li, S.; Zhang, W.; Peng, K. Influence of processed parameters on the magnetic properties of Fe/Fe$_3$O$_4$ composite cores. *J. Mater. Sci. Mater. Electron.* **2020**, *32*, 1233–1241. [CrossRef]

26. Huang, Z.; Huang, H.; He, H.; Wu, Z.; Wang, X.; Wang, R. Effect of Various Metal Oxide Insulating Layers on the Magnetic Properties of Fe-Si-Cr Systems. *Coatings* **2023**, *13*, 804. [CrossRef]

27. Hsiang, H.; Wang, S.; Chen, C. Electromagnetic properties of FeSiCr alloy powders modified with amorphous $SiO_2$. *J. Magn. Magn. Mater.* **2020**, *514*, 167151. [CrossRef]

28. Guo, R.; Yu, G.; Zhu, M.; Qiu, Y.; Wu, G.; Zhou, H. Regulation of magnetic and electrical performances in core- shell-structured FeSiCr@BaTiO$_3$ soft magnetic composites. *J. Alloys Compd.* **2022**, *895*, 162724. [CrossRef]

29. Yu, H.; Zhou, S.; Zhang, G.; Dong, B.; Meng, L.; Li, Z. The phosphating effect on the properties of FeSiCr alloy powder. *J. Magn. Magn. Mater.* **2022**, *552*, 168741. [CrossRef]